Next Materials 12 (2026) 102323

Contents lists available at ScienceDirect

Next Materials

journal homepage: www.sciencedirect.com/journal/next-materials

Research article

Geochemical insights into ancient burnt clay bricks in Sri Lankan archaeological structures

K.D.H.J. Premarathne [a,b,*], Sansfica M. Young [c], T. Mendis [d], M. Rajapaksha [e], J.M.I.R.K. Jayasekara [d], R.U. Halwatura [b], A. Kamei [f]

[a] Department of Architecture, General Sir John Kotelawala Defence University, Sri Lanka
[b] Department of Civil Engineering, University of Moratuwa, Sri Lanka
[c] Department of Environment Technology, University of Colombo, Sri Lanka
[d] Department of Archaeology and Heritage Management, Rajarata University, Sri Lanka
[e] School of Architecture, Sri Lanka Institute of Information Technology, Sri Lanka
[f] Department of Earth Science, Interdisciplinary Faculty of Science and Engineering, Shimane University, Japan

ARTICLE INFO

Keywords:
Ancient burnt clay bricks
Geochemical signature
Compressive strength
Firing technology
XRF
SEM-EDX

ABSTRACT

Ancient burnt clay bricks in Sri Lanka exhibit comparatively advanced technological characteristics relative to many contemporary clay bricks (1–5 MPa), suggesting the presence of optimized material design principles. This study investigates the geochemical signatures and structure–property relationships of ancient clay bricks with relatively high compressive strengths to derive insights relevant to the development of sustainable modern construction materials. Ancient burnt clay bricks were collected from ten stupas located in Anuradhapura, Sri Lanka. Standard methods were used to test the compressive strength of the brick samples. Advanced materials characterization techniques, including X-ray fluorescence (XRF), scanning electron microscopy (SEM) coupled with energy-dispersive X-ray spectroscopy (EDX) and X-ray diffraction (XRD) were employed to analyze the geochemical signatures. The data were analyzed to explore provenance trends, relative weathering alteration, chemical composition, mineralogical phases, and possible firing temperature ranges of the ancient burnt clay bricks. The provenance analysis is broadly consistent with relatively felsic source materials of dacitic to rhyolitic affinity. A significant correlation was identified between flux content (19.56%) and compressive strength (9.78 MPa), suggesting that vitrification and densification may have contributed to improved mechanical performance. Further, the bricks are consistent with production from non-calcareous, low-refractory clays (CaO < 6%), with flux levels exceeding 9%, which may have supported effective sintering during firing. The higher-strength burnt clay bricks likely experienced comparatively higher firing temperatures, as indicated by the possible presence of high-temperature mineral phases such as mullite and diopside. SEM-EDX results suggest that the morphology and elemental distribution patterns of the clay bricks may have contributed to higher compressive strength. Overall, the findings suggest that ancient brick production involved favorable material characteristics and firing conditions, providing a useful basis for the development of next-generation sustainable clay-based construction materials.

1. Introduction

Burnt clay bricks remain one of the most widely used construction materials worldwide due to their availability, durability, and cost-effectiveness [1,2]. Despite their widespread use, modern clay bricks often exhibit moderate mechanical performance and durability, creating a growing interest in improving their material efficiency and sustainability. Understanding ancient burnt clay brick technology provides a valuable pathway for developing optimized and sustainable construction materials.

Brickwork has been used as a structural material since ancient times, with civilizations employing it for thousands of years [3,4]. Sri Lankan ancient structures have exhibited remarkable durability over centuries, indicating the effectiveness of ancient brick manufacturing technologies. According to Prematilleke [5], the introduction of burnt clay bricks in Sri Lanka was largely influenced by early Indian architectural

* Corresponding author at: Department of Architecture, General Sir John Kotelawala Defence University, Sri Lanka.
E-mail address: kdhjpremarathne@kdu.ac.lk (K.D.H.J. Premarathne).

https://doi.org/10.1016/j.nxmate.2026.102323
Received 8 March 2026; Received in revised form 19 May 2026; Accepted 19 May 2026
Available online 26 May 2026

practices, which were brought to the island by Buddhist missionaries. The durability of these bricks made them ideal for constructing religious monuments such as stupas, which required materials capable of withstanding harsh environmental conditions. However, Gamlath [6] emphasized that there are no high-quality ancient burnt clay structures in India. Similarly, Deraniyagala [7] suggested that excavations at the Anuradhapura citadel revealed the earliest evidence of burnt brick usage in Sri Lanka, dating back to the 3rd century BC.

In Sri Lanka, monumental structures such as the Jetavanaramaya Stupa in Anuradhapura and Rankoth Vehera in Polonnaruwa represent some of the most significant examples of ancient brick construction. The Jetavana Stupa, standing at 122 m in height, is the tallest brick structure in the world, and the third tallest structure in the world [8]. Ranaweera and Aberuwan [9] and Gunasinghe and Karunarathna [10] emphasized that the construction materials utilized in the stupa must adhere to high-quality standards, particularly emphasizing the good compressive strength, as the main load acting on the stupa is its self-weight. Previous studies have reported that ancient Sri Lankan bricks exhibit higher compressive strength (8.5–11.6 MPa) compared to many modern bricks (0.95–5.3 MPa) [9,10]. In addition, Gunasinghe and Karunarathne [10] found that ancient bricks have one-tenth the material removal rate of modern bricks, indicating that the wear resistance of ancient bricks is ten times higher than that of modern bricks.

The performance of burnt clay bricks is primarily governed by the chemical composition of the raw materials, firing temperature, and mineralogical transformations occurring during firing. The chemical properties and the chemical composition play a critical role in determining the durability and strength of a brick. The formation of high-temperature phases and vitrified structures significantly influences strength, porosity, and durability [11–13]. The production of bricks involves complex chemical reactions occurring at various temperature ranges during firing; understanding these reactions is essential for optimizing key properties such as strength, durability, and porosity [14]. Previous studies have shown that increasing firing temperature can reduce porosity and enhance densification, thereby improving mechanical performance [15]. However, most existing research on ancient bricks has focused on individual aspects such as compressive strength and durability, without establishing a comprehensive understanding of how these factors interact.

Despite these contributions, a critical gap remains in understanding the combined influence of geochemical composition, firing-induced phase evolution, and microstructural development on the mechanical performance of ancient burnt clay bricks. In particular, the mechanisms governing the superior compressive strength of ancient bricks compared to modern counterparts have not been systematically explained through an integrated framework. Thus, the novelty of this study lies in the integrated interpretation of geochemical signatures, firing-induced mineral phase evolution, microstructural characteristics, and compressive strength of ancient Sri Lankan burnt clay bricks.

Therefore, this study aims to investigate the geochemical characteristics, mineralogical phase evolution, and microstructural features of ancient burnt clay bricks from the Anuradhapura archaeological complex, and to establish relationships between chemical composition and mechanical performance. The primary objective of this research is to investigate the chemical composition, provenance, weathering patterns, firing technology, material formations, and morphology based on the geochemistry of the ancient burnt clay bricks that may contribute to their high strength, quality and durability.

The findings of this study provide scientifically grounded insights into flux-controlled vitrification, high-temperature phase formation, and microstructural densification mechanisms of ancient bricks. These insights establish a scientific foundation for developing optimized material design strategies and advancing sustainable clay-based construction materials by translating historically proven technologies into modern engineering applications.

2. Materials and methods

2.1. Materials

Anuradhapura was the first prominent ancient capital of Sri Lanka, with a rich history, culture, and architectural heritage. Many stupas, including the famous Ruwanwelisaya and Jetavana stupas, were constructed in Anuradhapura [9]. Sampling bricks from these historical sites offers insights into the prevalent brick-making techniques and materials used during that period.

Ancient burnt clay brick samples were collected from selected stupas within the Anuradhapura region. The physical, chemical, and mineralogical changes in soil at specific geographical locations significantly influence the properties of bricks [16]. Thus the sampling strategy was designed to capture variation across structural zones of the stupas, namely the core, middle, and periphery layers (Fig. 1). A total of ten (10) ancient stupas in the Anuradhapura region were selected for sampling based on literature evidence of timeline, historical significance, and the availability of exposed brick materials suitable for non-destructive extraction.

The selected stupas represent a broad chronological range spanning from approximately the 3rd century BCE to the 3rd century CE. Early constructions include Kiribath Vehera (307 BCE), Kadahatha Stupa and Wadakahagalahinna Stupa (300 BCE – 100 CE). Intermediate phase structures include Abhayagiri Stupa (89–77 BCE), Anula Stupa (161–137 BCE), Mihindu Seya (c. 140 BCE), and Nawagala Stupa (161–131 BCE). Later constructions such as Kulumeemakada Stupa (200 CE), Jetavanaramaya Stupa (273–301 CE), and Kiralagala Stupa (300 CE) represent more advanced phases of ancient Sri Lankan brick construction.

Within the stupa's construction, burnt clay bricks are strategically placed according to brick size and strength. The highest compressive strength bricks were found in the foundation, the outer cover of the dome, and the third basal ring of the the upper basal rings of the each stupas. Therefore, collected samples represent variation across structural zones and stupa [10]. Number of seventeen samples (Fig. 2) were collected from the dome and selected monuments, rather than a complete representation of all bricks used within each stupa.

2.2. Methods

2.2.1. X-ray fluorescence (XRF) analysis

Brick fragments were randomly collected and crushed to a fine powder using an automatic agate (RETSCH-RM200) and pestle grinder. Seventeen ancient burnt brick samples and Galkadawala soil samples were grinded and made to powder and 50 g from each sample was stored in polythene bags. The powdered (< 63 μm) brick samples were compressed using a force of 200 kN for 60 s. The concentrations of a total of ten major oxides (SiO_2, TiO_2, Al_2O_3, Fe_2O_3, MnO, MgO, Na_2O CaO, K_2O and P_2O_5) and fifteen trace elements (As, Cr, Cu, Nb, Ni, Pb, Rb, Sc, Sr, Th, V, Y, Zn, Zr and S) were then determined by X-ray fluorescence spectrometry using a Rigaku ZSX PRIMUSIV spectrometer at Shimane University, Japan which facilitated the precise determination of these concentrations with an average relative error of ±8%.

2.2.2. X-ray diffraction (XRD) analysis

X-ray diffraction (XRD) analysis was performed on a selected three ancient burnt clay bricks, chosen based on its notably compressive strength ranges, to determine its mineralogical composition. Powdered sample was compressed onto the sample holder and the X-ray diffraction pattern was recorded under the following conditions: Cu-Kα radiation (1.54 Å), a voltage of 40 kV, a current of 40 mA, 2θ range from 5° to 90°, an increment of 0.02° and a scan speed of 10 Deg/Min. Analytical instruments was calibrated using standard reference materials prior to measurement.

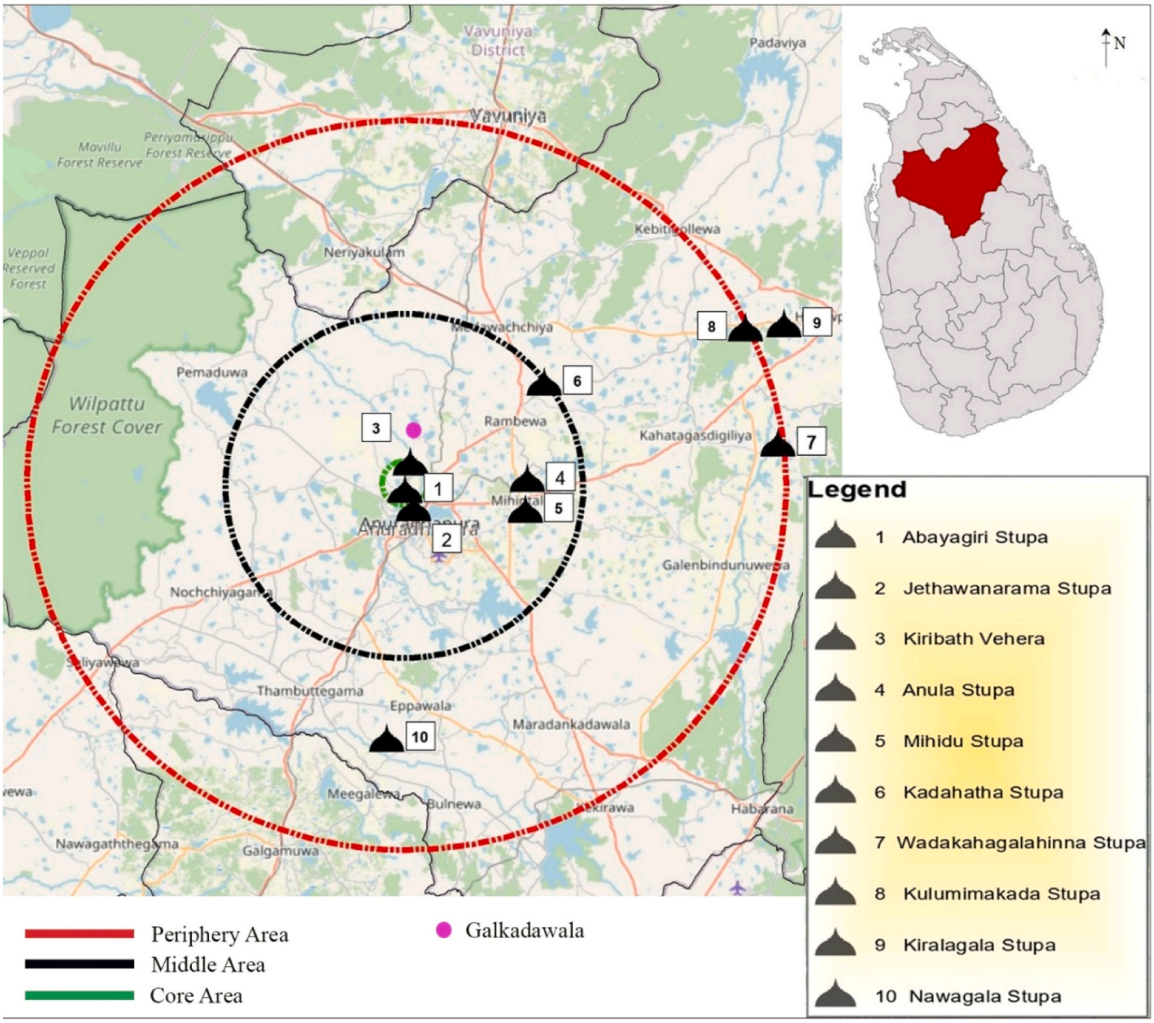

Fig. 1. Geographical locations of the stupas in Anuradhapura- Core area, Middle area and Periphery area.

2.2.3. *SEM–EDX analysis*

Scanning electron microscopy coupled with energy-dispersive X-ray spectroscopy (SEM-EDX) was employed to qualitatively examine the microstructural changes and the corresponding elemental distribution of the brick samples. Representative samples (JE1, KB1, NA1, and KA3) were selected based on their compressive strength.

A small, smooth cross-section representing the brick fragment was removed from the bulk and mounted into the SEM holder using a double-sided conductive adhesive tape and then coated with a thin layer of gold (SC7620 Sputter Coater). The SEM image (1,000x, 2,000x, and 4,000x magnification) was obtained using the EVO18 SEM/EDX instrument.

Complementary observations were conducted using a compound light microscope to examine the surface morphology, particle distribution, and visible pore characteristics of the brick samples. Prepared cross-sectional surfaces were observed under magnifications ranging from 40 × to 100 × to identify microstructural features such as matrix heterogeneity.

2.2.4. *Compressive strength testing*

Compressive strength testing procedure was performed according to the BS EN 772–1: [17] standards. Lourenco et al. [18] has described sample preparation of old brick for the compression test; the specimens were cut from the bricks in the moulding direction. Accordingly, number of three specimes were tested from each sample. Prior to testing, the loading surfaces of the brick specimens were prepared by capping to ensure smooth, plane, and parallel faces, which is essential for achieving reliable and reproducible compressive strength results. The results were reported as mean compressive strength values with corresponding standard deviations.

3. Results and discussion

3.1. *Provenance identification*

The Zr/Sc and Th/Sc ratios widely used for the identification of provenance in sedimentary geochemistry, while Th/Sc ratio reflects the bulk composition of the source, and Zr/Sc ratio is used to recognize heavy mineral concentrations [21]. These approaches have also been applied in archaeometric studies, where the chemical composition of ceramics is used to infer the provenance of raw clay materials [22,23]. In addition, previous studies have suggested that trace element compositions are largely preserved during the firing of clay, allowing fired ceramic materials, including bricks, to retain geochemical signatures indicative of their original clay sources [24]. Therefore, observed trends provide insights into the dominant compositional signatures and potential provenance of the raw materials used in ancient brick production.

According to Fig. 3(a), ancient clay brick samples belonging to core area, middle area and periphery area of Anuradhapura fall within the range between dacite (DAC) and rhyolite (RH) in compositional range, which is broadly consistent with a relatively felsic source affinity. The

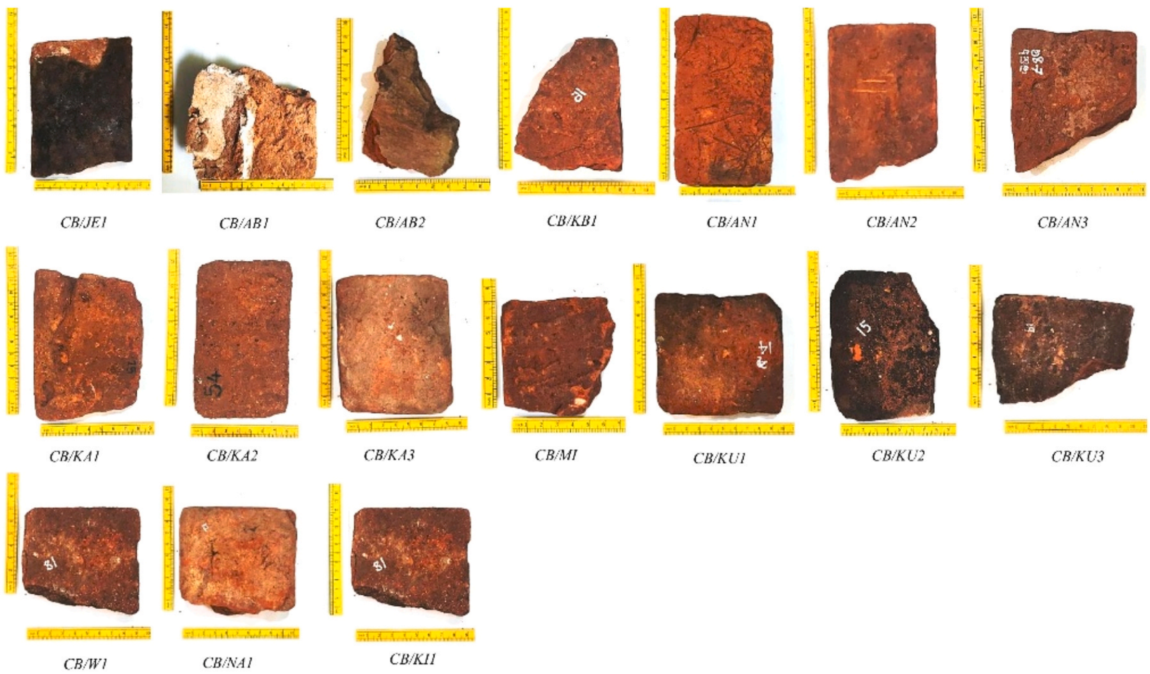

Fig. 2. Collected ancient burnt clay brick samples from the stupas in Anuradhapura.

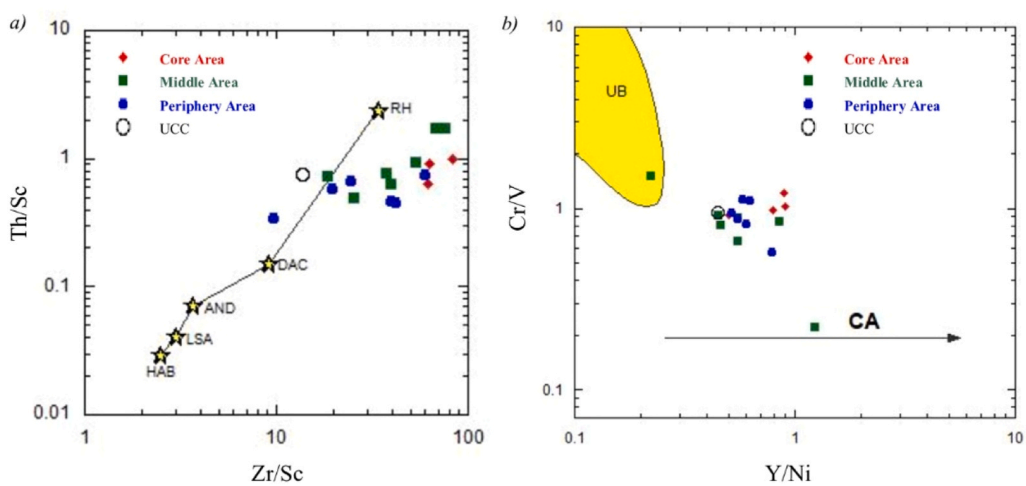

Fig. 3. a) Zr/Sc–Th/Sc ratio plots [20] for ancient burnt clay bricks, b) Cr/V–Y/Ni plots [20] for acient clay bricks in the core, middle and periphery area of Anuradhapura.

average Th/Sc ratios for the core, middle, and periphery areas are 0.85, 1.01, and 0.54, respectively, compared with the Upper Continental Crust (UCC) value of 0.75 [19]. The corresponding average Zr/Sc ratios are 72.5, 45.4, and 32.3, respectively, whereas the UCC value is 13.78 [19]. These elevated Zr/Sc ratios may reflect relative Zr enrichment and possible heavy mineral concentration, particularly in the core area. However, the scattered distribution of samples across all three structural zones suggests some compositional variability within an overall felsic tendency. Further, this interpretation is supported by the Chemical Weathering Index (CIA), which highlights variations in the degree of weathering and geochemical conditions across the sampled areas.

Similarly, Cr/V and Y/Ni ratios reflect preferential concentration of chromium over other ferromagnesian elements [20,25]. The Cr/V–Y/Ni plot (Fig. 3(b)) shows that most samples cluster within a compositional field consistent with felsic sources.The average ratio of Cr/V is 1.03, 0.83 and 0.91 and Y/Ni ratio is 0.77, 0.61, and 0.61 in core area, middle area and periphery area, respectively. These values are generally consistent with a felsic tendency. One middle-area sample (KA2) plots closer to an ultrabasic compositional field, likely due to its relatively high Cr content (129 ppm) and lower V content (85 ppm) compared with the other samples. In contrast, sample KA1 plots within a felsic calc-alkaline field and is characterized by lower Cr (23 ppm) and V (103 ppm) concentrations.

The felsic tendency indicated by the Zr/Sc–Th/Sc and Cr/V–Y/Ni relationships suggests that ancient brickmakers may have used clay sources rich in silica–alumina components with suitable heavy mineral contributions. Such raw material characteristics may have supported the formation of stable ceramic matrices during firing and contributed to the long-term performance of the bricks.

3.2. Variation with crustal composition of clay

According to Fig. 4, the core area samples show the most stable patterns, with fewer extreme enrichment and depletion. The middle area

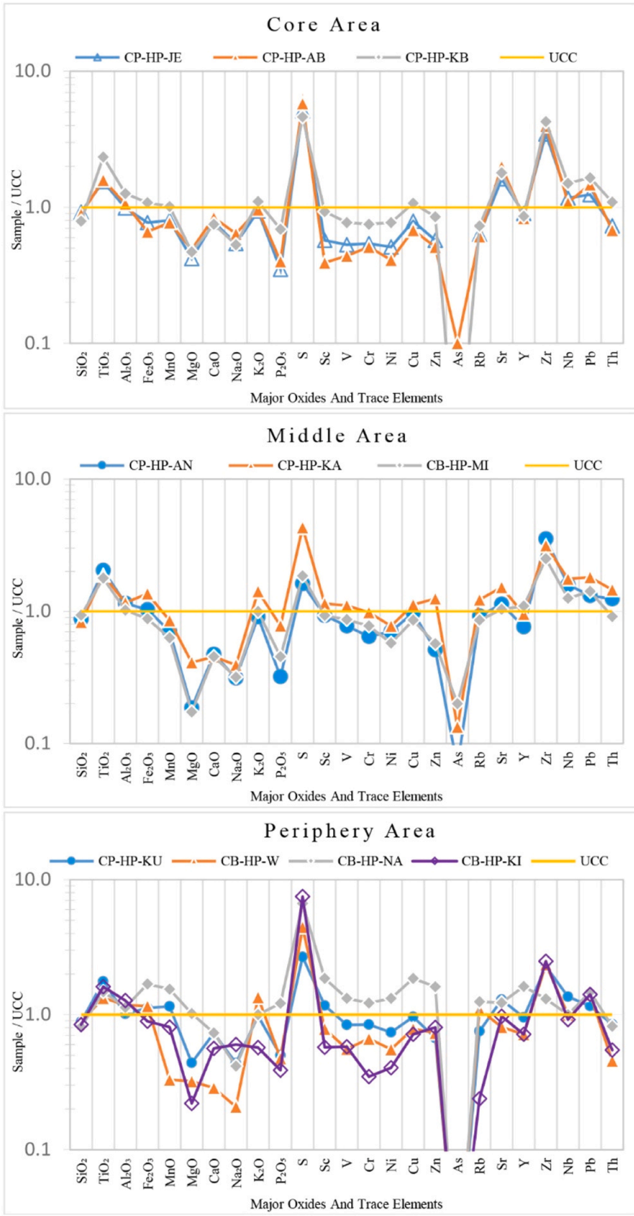

Fig. 4. Average normalized samples compared to average Upper Continental Crust (UCC) normalized values from Rudnick & Gao, [19]. The major element values were normalized as wt%. The trace element values were normalized as ppm, *a)samples from core area, b) middle area, c) periphery area of Anuradhapura.*

exhibits moderate variability, reflecting its transitional nature. The periphery area shows the highest variability and extreme enrichment and depletion trends, likely influenced by external environmental conditions.

The concentrations of major oxides closely align with the Upper Continental Crust (UCC) except for TiO_2 (average core - 1.13, middle - 1.24, periphery - 1.03, UCC - 0.64) enrichment and depletion of MgO (average core - 1.16, middle - 0.69, periphery - 1.19, UCC - 2.48) Na_2O (average core - 1.92, middle - 1.14, periphery −1.38, UCC - 3.27) and CaO (average core - 2.88, middle - 1.66, periphery - 2.25, UCC - 3.59) in all three areas.

However, in terms of trace elements such as As, Zr, and Sr, there are pronounced deviations from the UCC values. Arsenic shows depletion, while Sr and Zr show enrichment in all samples. The relative enrichment of Zr and Sr may reflect their greater persistence during firing and apparent concentration effects associated with the loss or transformation of other components at elevated temperatures. Further, sulfur shows enrichment in every ancient brick sample compared to the UCC values.

3.3. *Weathering and alteration trends of the ancient bricks*

Various indices for assessing weathering are documented in the literature, with the most commonly utilized one being the Chemical Index of Alteration (CIA = $Al_2O_3/(Al_2O_3 + CaO^* + Na_2O + K_2O)$], with CaO* representing the adjusted concentration of CaO) [26]. The CaO* value was calculated following the method proposed by McLennan et al. [20], in which calcium associated with apatite is corrected using the relationship: $CaO^* = CaO - (10/3 \times P_2O_5)$. The CIA has been integrated into the A-CN-K compositional diagram, enabling effective evaluation of chemical weathering, diagenesis, metamorphism, and source composition [27]. Although the CIA and A–CN–K indices were originally developed for unaltered sediments and rocks, previous studies have shown that these geochemical indices can be applied to archaeological ceramics to assess compositional variations and alteration trends [28, 29]. Therefore, the CIA-based interpretations are presented as indicative of relative trends rather than absolute measures of weathering intensity.

Fig. 5 illustrates the distribution of brick samples in the A-CN-K ternary diagram, particularly their proximity to the "A" vertex, which can provide a relative indication of weathering trends and compositional variations. CIA values near 50 indicate minimal weathering, around 75 reflect moderate alteration, and close to 100 signify intense chemical alteration with significant leaching of mobile elements [30]. Accordingly, the CIA value of brick samples collected from the core area vary between 57.9 – 64.1 (Average 59.8), in the middle area 63.6 – 74.3 (Average 68.6), and CIA values in the periphery area samples vary between 64.4 – 72.5 (Average 65.1). These results suggest relatively lower geochemical alteration in core area samples compared with those from the middle and periphery areas.

Less altered brick such as JE1, AB1, KU1, KU2, and KA3, indicates comparatively high flux content. The most weathered brick (CIA= 74.27) sample is from the Anula stupa (AN2) located in the middle area of Anuradhapura and shows the lower flux (9.52) content and average compressive strength. This suggests that bricks with relatively lower flux content may experience reduced vitrification, potentially resulting in a more open and porous microstructure. Such characteristics can facilitate water absorption and increase susceptibility to weathering processes [16,31]. Samples with lower alteration and higher flux content may

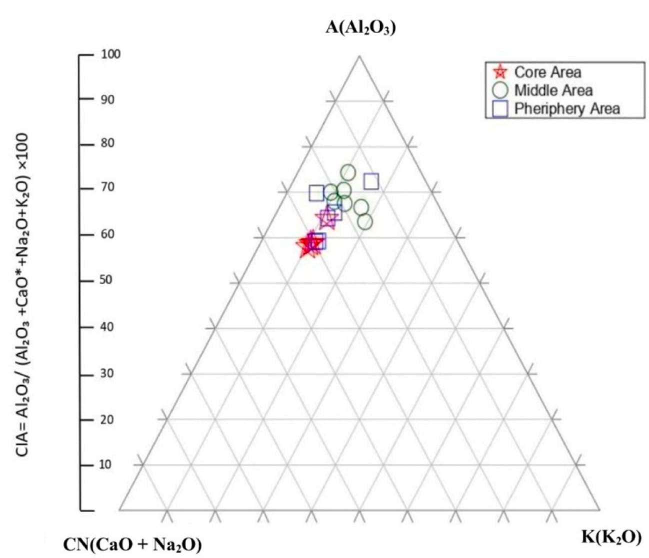

Fig. 5. Distribution of analyzed samples in the A-CN-K (Al_2O_3-CaO + Na_2O-K_2O) ternary diagram, [26] with calculated CIA values.

have undergone more effective vitrification, reducing open porosity and improving resistance to moisture-related deterioration.

3.4. Chemical composition, flux content and compressive strength

Table 1 indicates that the KA3(Kadahatha) sample exhibits the highest compressive strength (9.78 MPa). This comparatively high strength may be related to its chemical composition and mineralogical characteristics. The sample has the lowest SiO_2 content (47.98%), indicating a reduced presence of quartz, which typically acts as an inert filler in clay matrices and contributes less directly to densification during firing [32]. In contrast, KA3 contains comparatively higher Fe_2O_3 (8.12%), which has been reported to act as a fluxing component and may promote vitrification by lowering the effective melting temperature of the system [33].

Relatively elevated concentrations of MnO (0.13%), V (133 ppm), Cr (118 ppm), Cu (61 ppm), Zn (152 ppm), Rb (176 ppm), and Sr (274 ppm) compared to other samples suggests that these transition metal oxides contribute to glass phase formation, improving sintering and reducing porosity [34,35]. Previous ceramic studies have suggested that zinc oxide (ZnO) promotes the formation of cristobalite while copper oxide (CuO) and vanadium oxide (V_2O_5) reduce the temperature of mullite formation [36–38]. Additionally, the high alumina content (Al_2O_3 19.39%) improves structural integrity by forming mullite ($Al_6Si_2O_{13}$) at high temperatures, which enhances mechanical strength and durability [39]. The combined presence of increased fluxing oxides (Fe_2O_3, CaO, Na_2O, and K_2O), sufficient Al_2O_3, and metal oxide constituents may have contributed to improved densification, reduced porosity, and the comparatively high compressive strength of the KA3 sample.

Ravisankar et al. [40] emphasized that if the flux concentration (K_2O, Fe_2O_3, CaO, MgO, and TiO_2) is more than 9%, the clays are classified as low refractory, and they are classified as high refractory if the fluxes in the sample are less than 9%. The total flux content was determined using the formula,

Total Flux Content $= RO + R_2O + Fe_2O_3 + TiO_2$, where $RO = CaO + MgO$ and $R_2O = K_2O + Na_2O$ [41,42].

According to Table 1, flux concentration in all brick samples of core, middle and periphery areas exceeding 9% indicates that they can be classified as low refractory clays. This classification stems from the presence of fluxing oxides such as K_2O, Fe_2O_3, CaO, MgO, and TiO_2, which lower the melting point of the material, thereby reducing its refractoriness. The highest flux content is shown by the KA3 brick (18.1%) which also indicates the highest compressive strength. Riccardi et al. [33] stated that flux content variation affects phase transitions, altering mechanical strength. Further, Table 1 shows that the content of the CaO in all samples less than 6%, which classifies the raw clay as non-calcareous [34].

According to Fig. 6, samples with flux content > 15%, such as CP-HP-KA3 (19.56%) and CP-HP-KU3 (15.54%), exhibit the highest compressive strengths (9.78 N/mm^2 and 8.06 N/mm^2), respectively. This trend is broadly consistent with previous studies indicating that flux-rich, low-refractory clays may promote vitrification and glassy phase development at relatively lower firing temperatures, which can contribute to reduced porosity and improved mechanical performance [33,41,43]. For example, the relatively high Fe_2O_3 content of KA3 (8.12%) may have promoted sintering, while its Al_2O_3 content (19.39%) may have favored the development of thermally stable aluminosilicate phases under suitable firing conditions [44]. Conversely, the low concentration of fluxing oxides limits the formation of mullite and cristobalite phases during the vitrification process at higher temperatures, thereby resulting in lower densification and a subsequent decrease in the mechanical strength of the clay-based product [45].

Although higher flux content generally improves compressive strength, several samples deviate from this trend, indicating that additional factors also influence strength development. For instance, CB-KB1 (15.60% flux, 2.68 MPa), CB-KI1(11.65% flux, 3.52 MPa), and CB-AB1 (14.22% flux, 3.60 MPa), exhibit remarkably low strength despite moderate flux levels. Furthermore, CB-NA1 (18.76% flux, 5.66 MPa), CB-KA1 (18.0% flux, 6.17 MPa) and CB-KU2 (15.81% flux, 5.66 MPa) show moderate strength with higher flux content. These samples were compared with the bricks of similar flux content and higher compressive strength. The results suggest that flux content of the KB1, AB1 and KI1 is predominantly contributed by CaO, K_2O and Na_2O. This indicates that the type and balance of fluxing oxides are critical. Potassium oxide and Sodium Oxide are alkaline fluxes, where excessive amounts lead to over-vitrification, producing weak amorphous matrices and reducing mechanical integrity [42,46]. Similarly, excess CaO content may results in unstable hydraulic phases, which negatively affect durability and mechanical integrity [32,41,46]. Despite a high flux content, inadequate microstructural bonding or increased porosity may reduce the compressive strength of clay bricks [47,48].

These results indicate that flux content alone does not fully control compressive strength. Instead, strength development appears to depend on the combined effects of flux-assisted vitrification, high-temperature mineral phase formation, pore structure, and particle bonding [49]. Therefore, high-temperature mineral phase formation, XRD-based mineralogical evidence, and SEM-observed microstructural densification interpreted together in following sections.

3.5. Firing technology and mineralogical phase development

Compared to modern brick manufacturing processes, which often involve lower firing temperatures and less controlled raw material composition, the ancient bricks studied here appear to exhibit more optimized material characteristics. Modern bricks typically show compressive strengths in the range of 1–5 MPa [9], whereas the ancient samples demonstrate significantly higher values. This suggests that ancient brick production may have achieved improved densification through a favorable combination of raw material selection and firing conditions [44–50]. Table 1 presents the chemical composition of burnt clay bricks from the three study areas together with the Galkadawala soil sample, which is considered here as a possible representative raw material analogue for ancient brick production. Compared to the brick samples (average Al_2O_3 - 17.13%, Fe_2O_3 - 5.43%) and soil sample the concentrations of Al_2O_3 and Fe_2O_3 have increased (Al_2O_3 - 14.11%, Fe_2O_3 - 3,56%) during the firing process, whereas MgO and CaO have experienced acceptable reductions in all ancient brick samples (average brick samples MgO - 0.98%, CaO - 2.16%, Soil sample MgO - 3.54%, CaO - 7.12%). These compositional differences may reflect firing-induced mineral decomposition, volatilization, and phase transformation processes at different firing ranges.

Aluminium oxides are derived from aluminosilicate minerals such as kaolinite and illite. Clay minerals in the raw soil, such as kaolinite undergo dehydroxylation and structural reorganization at high temperatures, leading to the formation of phases like mullite ($Al_6Si_2O_{13}$) and hematite (Fe_2O_3) [48]. At temperatures of 800 °C to 850 °C, significant chemical reactions involving illite and calcite occur, producing various silicate phases such as gehlenite, which contribute to the durability of the bricks [51]. The transformation of clay minerals at this stage is crucial for achieving the desired mechanical properties. Formation of various silicate phases and their possible stoichiometric can be illustrated according to the firing temperature as follows;

$2KAl_2(Si_3Al)O_{10}(OH)_2 + 6CaCO_3 \rightarrow 3Ca_2Al_2SiO_7 + 3SiO_2 + K_2O + 2H_2O + 6CO_2$ (800 °C - 850 °C)

illite calcite gehlenite

$CaCO_3 + 2SiO_2 + 2KAlSi_3O_8 \rightarrow CaAl_2Si_2O_8 + K_2O + 6SiO_2 + CO_2$

calcite K-feldspar anorthite

Table 1
Elemental concentration of major oxides (%) and trace elements (ppm), Upper Continental Crust (UCC) [19] Chemical Index Alteration (CIA), compressive strength, flux content and Loss of Ignition (LOI) of the relevant bricks.

Sample	SiO_2 mass %	TiO_2 mass %	Al_2O_3 mass %	Fe_2O_3 mass %	MnO mass %	MgO mass %	CaO mass %	Na_2O mass %	K_2O mass %	P_2O_5 mass %	S ppm	Sc ppm	V ppm	Cr ppm	Ni ppm	Cu ppm	Zn ppm	As ppm	Rb ppm	Sr ppm	Y ppm	Zr ppm	Nb ppm	Pb ppm	Th ppm	CIA	Compressive Strength (MPa)	Flux Content	LOI
Core Area																													
CB-JE1	61.23	0.98	15.30	3.89	0.08	1.03	2.80	1.78	2.64	0.05	41	8	51	50	24	22	38	0	53	519	19	665	14	21	8	58.73	7.39 ± 0.21	13.12	5.12
CB-AB1	58.99	0.96	16.71	3.69	0.08	1.49	3.09	2.30	2.69	0.08	35	11	49	50	21	22	39	0	52	658	19	681	12	25	7	57.94	3.60 ± 0.31	14.22	2.57
CB-AB2	59.59	1.08	15.87	3.00	0.07	0.93	2.97	1.88	2.66	0.05	29	0	36	44	18	16	30	1	50	614	16	851	14	25	8	58.50	6.88 ± 0.23	12.52	5.92
CB-KB1	52.82	1.50	19.34	5.43	0.10	1.17	2.68	1.74	3.09	0.10	60	13	75	69	36	30	57	-1	61	572	18	823	18	28	12	64.11	2.68 ± 0.15	15.60	4.55
Maximum	**61.23**	**1.08**	**19.34**	**5.43**	**0.10**	**1.49**	**3.09**	**2.30**	**3.09**	**0.10**	**60**	**13**	**75**	**69**	**36**	**30**	**57**	**1**	**61**	**658**	**19**	**851**	**18**	**28**	**12**	**64.11**	**7.39**	**16.48**	**5.92**
Minimum	**52.82**	**0.96**	**15.30**	**3.00**	**0.07**	**0.93**	**2.68**	**1.74**	**2.64**	**0.05**	**29**	**0**	**36**	**44**	**18**	**16**	**30**	**-1**	**50**	**519**	**16**	**665**	**12**	**21**	**7**	**57.94**	**2.68**	**11.94**	**4.55**
Average	**58.16**	**1.13**	**16.80**	**4.00**	**0.08**	**1.16**	**2.88**	**1.92**	**2.77**	**0.07**	**41.25**	**8**	**53**	**53.3**	**24.8**	**23**	**41**	**0**	**54**	**591**	**18**	**755**	**14.5**	**25**	**8.8**	**59.82**	**5.14**	**13.86**	**4.54**
Middle Area																													
CB-AN1	55.51	1.42	18.70	5.46	0.06	0.41	2.00	1.40	2.71	0.05	18	14	79	52	33	25	35	0	85	423	18	749	21	24	13	68.11	6.23 ± 0.29	13.40	6.84
CB-AN2	65.30	1.11	14.50	4.38	0.06	0.38	1.19	0.58	1.88	0.05	19	14	71	65	29	26	28	1	54	242	13	550	15	17	9	74.27	5.25 ± 0.47	9.52	8.43
CB-AN3	53.20	1.38	19.87	5.71	0.10	0.59	1.91	1.09	3.02	0.05	26	11	75	61	37	31	40	0	93	420	17	746	21	26	19	70.23	8.70 ± 0.44	13.70	5.04
CB-KA1	53.51	1.90	19.14	7.64	0.06	1.04	1.55	1.30	4.57	0.13	55	15	103	23	18	18	71	0	94	813	22	1143	37	30	26	66.59	6.17 ± 0.28	18.00	7.26
CB-KA2	64.11	0.65	14.96	4.77	0.06	0.32	1.58	1.10	1.77	0.06	31	10	85	129	36	15	27	1	38	373	8	254	8	18	5	69.88	5.63 ± 0.69	10.20	7.75
CB-KA3	47.98	1.06	19.39	8.12	0.13	1.69	1.74	1.44	5.50	0.16	120	23	133	118	55	61	152	1	176	274	30	426	18	44	17	63.55	9.78 ± 0.12	19.56	6.15
CB-MI	62.23	1.14	15.66	4.42	0.06	0.43	1.63	1.04	2.78	0.07	24	13	84	71	27	24	38	1	72	330	23	482	15	24	10	67.55	5.96 ± 0.34	11.43	9.06
Maximum	**65.30**	**1.90**	**19.87**	**8.12**	**0.13**	**1.69**	**2.00**	**1.44**	**5.50**	**0.16**	**120**	**23**	**133**	**129**	**55.00**	**61**	**152**	**1**	**176**	**813**	**30**	**1143**	**37**	**44**	**26**	**74.27**	**9.78**	**19.56**	**9.06**
Minimum	**47.98**	**0.65**	**14.50**	**4.38**	**0.06**	**0.32**	**1.19**	**0.58**	**1.77**	**0.05**	**18**	**10**	**71**	**23**	**18**	**15**	**27**	**0**	**38**	**242**	**8**	**254**	**8**	**17**	**5**	**63.55**	**5.25**	**9.52**	**5.04**
Average	**57.40**	**1.24**	**17.46**	**5.79**	**0.08**	**0.69**	**1.66**	**1.14**	**3.18**	**0.08**	**41.86**	**14.3**	**90**	**74.1**	**33.6**	**29**	**56**	**0.6**	**87**	**411**	**19**	**621**	**19.3**	**26**	**14**	**68.60**	**6.82**	**13.69**	**7.22**
Periphery Area																													
CB-KU1	62.01	1.34	15.51	5.03	0.09	0.39	1.85	1.31	2.59	0.07	30	15	72	80	32	18	34	0	55	341	20	590	20	18	7	65.54	5.61 ± 0.2	12.50	7.45
CB-KU2	55.86	0.96	16.35	5.79	0.12	1.43	3.13	1.53	2.98	0.09	50	15	85	81	37	32	49	0	69	451	19	365	14	21	10	59.30	5.40 ± 0.28	15.81	6.25
CB-KU3	58.84	1.07	14.90	6.07	0.14	1.45	2.86	1.46	2.63	0.07	51	19	87	72	35	31	52	0	66	448	21	369	15	20	11	59.21	8.06 ± 0.62	15.54	6.94
CB-WI	59.11	0.85	18.13	5.84	0.03	0.79	1.03	0.68	3.76	0.07	49	11	54	61	26	22	49	-1	92	259	15	456	12	24	5	72.47	6.45 ± 0.38	12.95	9.52
CB-NA1	53.94	0.94	17.39	8.50	0.15	2.53	2.63	1.36	2.80	0.18	173	26	128	112	62	52	108	0	105	391	34	252	12	25	9	64.41	5.66 ± 0.06	18.76	3.49
CB-KI1	56.24	1.03	19.60	4.50	0.08	0.55	2.02	1.96	1.60	0.06	60	8	56	32	19	20	54	0	20	311	15	479	11	24	6	69.79	3.52 ± 0.8	11.65	3.84
Maximum	**62.01**	**1.34**	**19.60**	**8.50**	**0.15**	**2.53**	**3.13**	**1.96**	**3.76**	**0.18**	**173**	**26**	**128**	**112**	**62**	**52**	**108**	**0**	**105**	**451**	**34**	**590**	**20**	**25**	**11**	**72.47**	**8.06**	**18.76**	**9.52**
Minimum	**53.94**	**0.85**	**14.90**	**4.50**	**0.03**	**0.39**	**1.03**	**0.68**	**1.60**	**0.06**	**30**	**8**	**54**	**32**	**19**	**18**	**34**	**-1**	**20**	**259**	**15**	**252**	**11**	**18**	**5**	**59.21**	**3.52**	**11.65**	**3.49**
Average	**57.67**	**1.03**	**16.98**	**5.96**	**0.10**	**1.19**	**2.25**	**1.38**	**2.72**	**0.09**	**68.83**	**15.7**	**80**	**73**	**35.2**	**29**	**58**	**-0.2**	**68**	**367**	**21**	**419**	**14**	**22**	**8**	**65.12**	**5.78**	**14.54**	**6.25**
CS-GA	54.94	1.14	14.11	3.56	0.10	3.54	7.12	1.33	2.17	0.03	0	56	17	12	23	20	42	1	639	7	65	18	33	495	111			18.85	8.10
Maximum	**65.30**	**1.90**	**19.87**	**8.50**	**0.15**	**2.53**	**3.13**	**2.30**	**5.50**	**0.18**	**173**	**26**	**133**	**129**	**62**	**61**	**152**	**0**	**176**	**658**	**34**	**1143**	**37**	**44**	**26**	**72.47**	**10.62**	**19.56**	
Minimum	**47.98**	**0.65**	**14.50**	**3.00**	**0.03**	**0.32**	**1.03**	**0.58**	**1.60**	**0.05**	**18**	**0**	**36**	**32**	**18**	**15**	**28**	**-1**	**20**	**242**	**8**	**252**	**8**	**17**	**5**	**57.94**	**2.68**	**9.52**	
Average	**57.67**	**1.14**	**17.13**	**5.43**	**0.09**	**0.98**	**2.16**	**1.41**	**2.92**	**0.08**	**51**	**13.3**	**78**	**68.8**	**32.1**	**27**	**53**	**0.2**	**73**	**438**	**19**	**581**	**16.3**	**24**	**11**	**65.30**	**6.06**	**14.03**	
UCC	**66.60**	**0.64**	**15.40**	**5.04**	**0.10**	**2.48**	**3.59**	**3.27**	**2.80**	**0.15**	**62**	**14**	**97**	**92**	**47**	**28**	**67**	**5**	**84**	**320**	**21**	**193**	**12**	**17**	**11**				

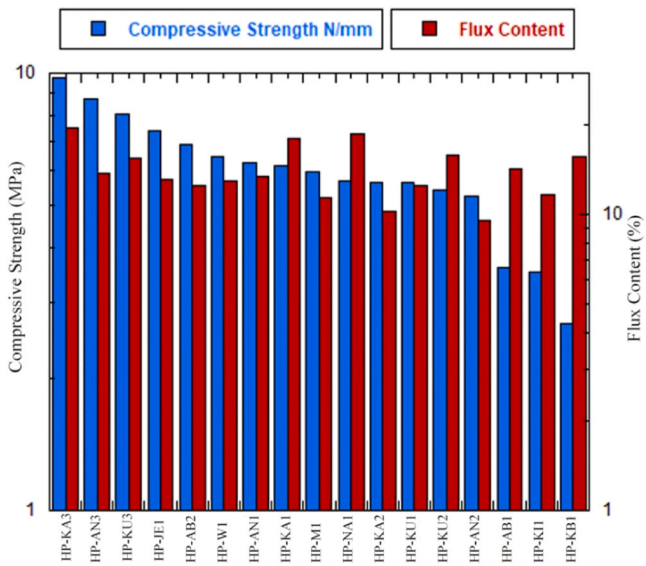

Fig. 6. Flux content and compressive strength of the burnt clay bricks.

$2Al_2O_3 + 4SiO_2 + 2CaCO_3 \rightarrow 2CaAl_2Si_2O_8 + 2CO_2$ (900 °C - 1000 °C)

calcite anorthite

Aluminum-bearing minerals are generally stable at firing temperatures 700–1200°C. Their decomposition into alumina-rich phases (e.g., mullite) results in an apparent enrichment [52]. Mullite is commonly identified at around 1000 ℃ - 1100 ℃ [50,53]. The appearance of mullite due to the epitactic replacement of muscovite as a result of the following reaction:

$3KAl_2(Si_3Al)O_{10}(OH)_2 + 2SiO_2 \rightarrow 3KAlSi_3O_8 + Al_6Si_2O_{13} + 3H_2O$ (1100 ℃)

illite/muscovite sanidine mullite

Similarly, wollastonite and diopside appear at 1100 ℃ as a reaction of quartz with calcite and dolomite [54]. The reactions form the wollastonite and diopside are as follows.

$SiO_2 + CaCO_3 \rightarrow CaSiO_3 + CO_2$

quartz calcite wollastonite

$2SiO_2 + CaMg(CO_3)_2 \rightarrow CaMgSi_2O_6 + 2CO_2$ (1100 ℃)

quartz dolomite diopside

Table 2 shows that the mole ratios of major oxides in the brick samples are broadly consistent with the stoichiometric requirements for the possible formation of silicate minerals such as gehlenite, anorthite, mullite, and diopside. This suggests that these silicate phases could have formed during the firing process, provided the necessary temperatures were achieved. The comparatively limited mole ratios of MgO and K_2O in the samples suggest limited formation of sanidine and diopside. In addition, the SiO_2 content of the ancient brick samples may have contributed to the ceramic framework during firing, while Al_2O_3 likely supported the development of thermally stable aluminosilicate phases, potentially including mullite under high-temperature conditions. Alumina enhances the plasticity of clay and forms mullite ($Al_6Si_2O_{13}$) during firing (1200 ℃), which is crucial for mechanical strength and durability [52].

Iron oxide (Fe_3O_4) is found in clay deposits, primarily in the form of hematite (Fe_2O_3) [55]. The decomposition of pyrite (FeS_2) occurs between 380 °C and 412 °C, resulting in the oxidation of iron, which imparts a characteristic red color to the bricks. This two-stage reaction leads to the formation of iron oxides, which gives aesthetic and physical characteristics of the clay bricks [56].

$FeS_2 + O_2 \rightarrow FeS + SO_2$ (380 °C - 412 °C)

$FeS + 7O_2 \rightarrow 2Fe_2O_3 + SO_2$

Table 2 suggests that presence of Fe-bearing minerals such as hematite that could form in all samples and the XRD patterns shown in Figs. 7–9 are consistent with the presence of hematite-bearing mineral.

MnO, MgO and CaO show significant reductions compared with the Galakadawala soil sample. Magnesium oxide (MgO) and calcium oxide (CaO) are often associated with carbonates such as dolomite ($CaMg(CO_3)_2$) and calcite ($CaCO_3$) in the raw clay or soil. During the firing process, these carbonates decompose at different temperatures, releasing carbon dioxide (CO_2) gas and leaving behind smaller amounts of residual oxides [57].

$CaMg(CO_3)_2 \rightarrow CaCO_3 + MgO + CO_2$

Dolomite calcite periclase

$CaCO_3 \rightarrow CaO + CO_2$ (600-900 ℃)

Calcite lime

$MgCO_3 \rightarrow MgO + CO_2$ (400-650 ℃)

Table 2
Calculated mole ratio of major oxides (derived from XRF data) in ancient brick sample and required ratio of oxides for mineral formation.

Sample	SiO_2: Al_2O_3:Fe_2O_3:MgO: CaO:K_2O mole ratio in sample						Required SiO_2: Al_2O_3: CaO mole ratio for Anorthite ($CaAl_2Si_2O_8$)			Required SiO_2: Al_2O_3:K_2O) mole ratio for Sanidine ($KAlSi_3O_8$)		
Core Area	SiO_2	Al_2O_3	Fe_2O_3	MgO	CaO	K_2O	SiO_2	Al_2O_3	CaO	SiO_2	Al_2O_3	K_2O
CB-HP-JE1	51	8	1	1	2	1	6	3	3	9	3	3
CB-HP-AB	49	8	1	2	3	1	Required SiO_2: Al_2O_3:CaO) mole ratio for Gehelenite ($Ca_2Al_2SiO_7$)			Required SiO_2:CaO:MgO) mole ratio for Diopside ($CaMgSi_2O_6$)		
CB-HP-KB1	29	6	1	1	2	1						
Middle Area												
CP-HP-AN	97	17	3	1	3	3						
CP-HP-KA	31	6	1	1	1	1	SiO_2	Al_2O_3	CaO	SiO_2	CaO	MgO
CB-HP-MI	104	15	3	1	3	3	3	3	6	2	1	1
Periphery Area							Required SiO_2: Al_2O_3 mole ratio for Mullite ($Al_6Si_2O_{13}$)			Required SiO_2: CaO mole ratio for wollastonite ($CaSiO_3$)		
CP-HP-KU	33	5	1	1	2	1						
CB-HP-WI	49	9	2	1	1	2						
CB-HP-NA1	30	6	2	2	2	1	SiO_2	Al_2O_3		SiO_2	CaO	
CB-HP-KI1	94	19	3	1	4	2	2	3		1	1	

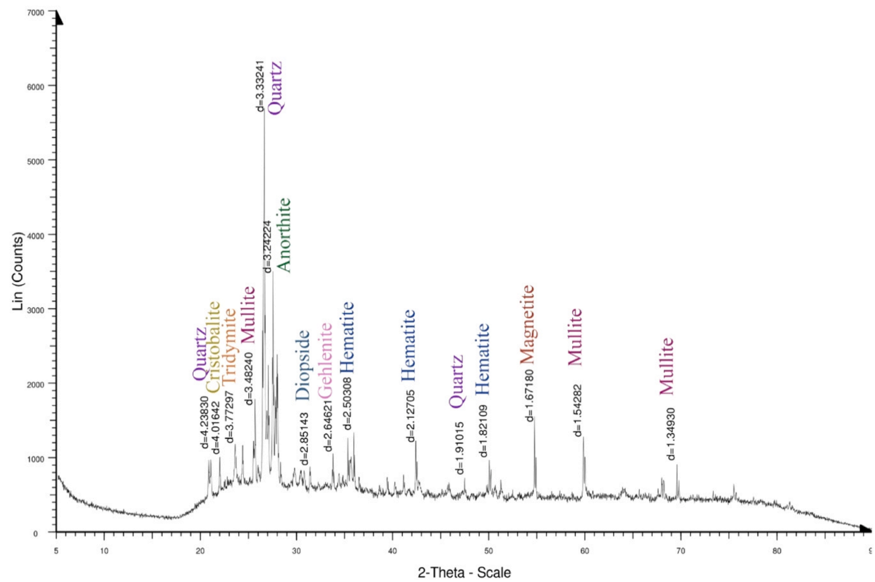

Fig. 7. X-ray Diffraction Curve of CB/KA3 ancient brick (9.78 MPa).

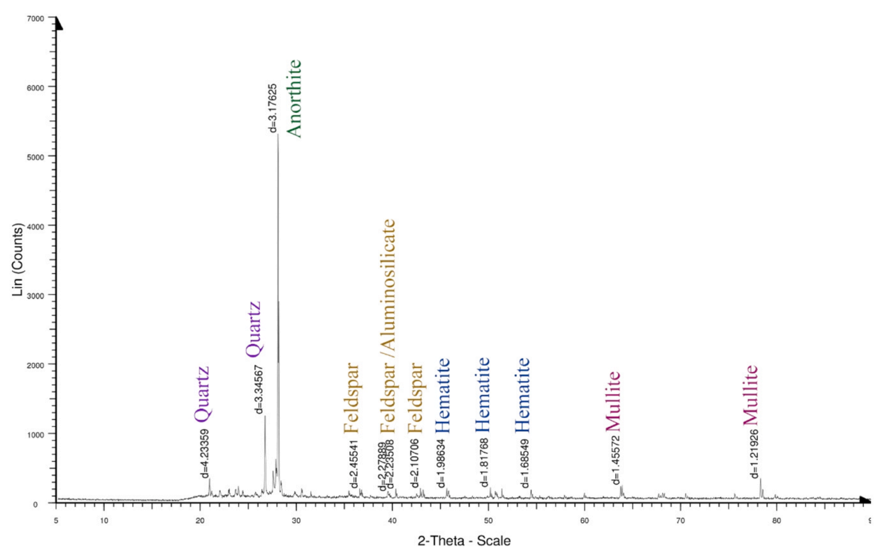

Fig. 8. X-ray Diffraction Curve of CB/JE1 ancient brick (7.39 MPa).

The decomposition of calcium carbonate ($CaCO_3$) into calcium oxide (CaO) at 800 °C also increases the porosity of the bricks, influencing their overall performance [58]. However, excess lime or magnesia can cause expansion, leading to cracking and lower strength [11]. Due to gas release during firing, the relative percentages of Al_2O_3 and Fe_2O_3 increase after firing.

Figs. 7, 8 and 9, the XRD curve of the CB/KA3, CB/JE1, and CB/KB1 brick samples evidence the formation of key crystalline phases such as quartz, anorthite, feldspar and hematite during firing. However, the compressive strength vary markedly, with KA3 showing the highest strength (9.78 MPa), followed by JE1 (7.39 MPa) and KB1 (2.68 MPa). This suggests that compressive strength may be influenced not only by the presence of quartz, but also by the extent of firing-induced mineral transformation and matrix densification. KA3 appears to contain a more advanced high-temperature mineral assemblage, including anorthite mullite, diopside, gehlenite, hematite, and magnetite, suggesting enhanced sintering and stronger interparticle bonding. JE1 also shows substantial mullite phase development, consistent with intermediate strength. In contrast, KB1, although containing quartz and anorthite, may have undergoneless effective densification and retained a weaker, more porous ceramic matrix, which explains its comparatively low compressive strength.

The data (Table 1) shows that the concentrations of yttrium, niobium, lead, rubidium, scandium, and thorium in the soil sample (soil – 65 ppm, 33 ppm, 495 ppm, 639 ppm, 56 ppm, 111 ppm respectively) are notably higher compared to the ancient burnt brick samples (average – 19 ppm, 16 ppm, 24 ppm, 73 ppm,133 ppm,11 ppm), whereas the concentrations of Sr, and Zr are comparatively lower in the soil sample (soil – 7 ppm, 18 ppm, average in ancient brick samples – 438 ppm, 581 ppm). The observed variation in elemental concentrations between the soil sample and the burnt brick samples can be attributed to the effects of the firing process and the transformation of minerals during brick production. Elements such as Y, Nb, Pb, Rb, Sc, and Th are commonly associated with refractory minerals, such as certain silicates, oxides, and phosphates [52,59]. These minerals exhibit high resistance to thermal decomposition and volatilization due to their strong crystal lattice structures and high melting points.

The XRF results provide clear evidence of Sr and Zr enrichment in the

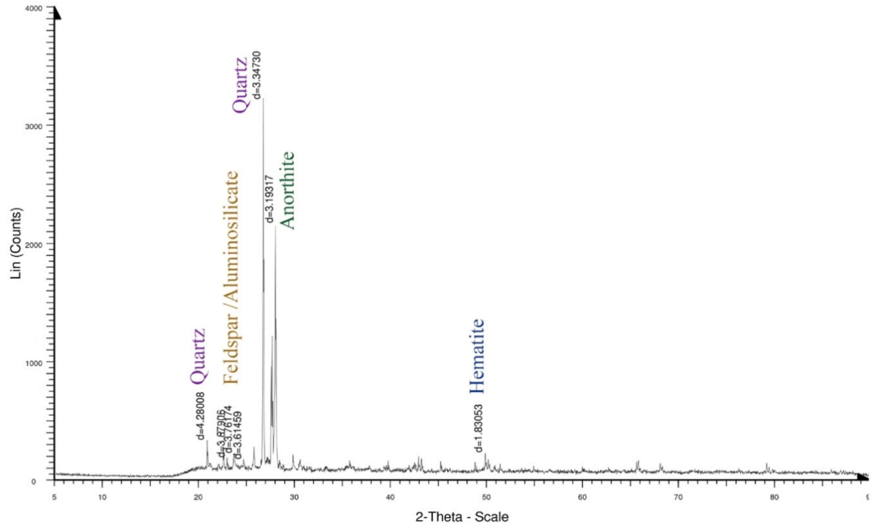

Fig. 9. X-ray Diffraction Curve of CB/KB1 ancient brick (2.68 MPa).

ancient burnt clay bricks relative to both the Galkadawala soil sample and average Upper Continental Crust composition. This enrichment may be attributed to the behaviour of Sr and Zr during the firing process and their association with thermally stable mineral phases. Strontium (Sr) is associated with calcium-rich minerals such as calcite or plagioclase feldspar, which decompose during firing to form new crystalline or amorphous phases that incorporate Sr [57,60]. Zirconium is primarily found in zircon ($ZrSiO_4$), a refractory mineral with a high thermal stability [52,57]. Therefore, the higher Sr and Zr contents in ancient bricks reflect both the mineralogical transformations during firing and the resilience of these elements and their host minerals under high-temperature conditions.

Similarly, sulfur enrichment is evident in the ancient burnt clay brick samples when compared with both the average Upper Continental Crust

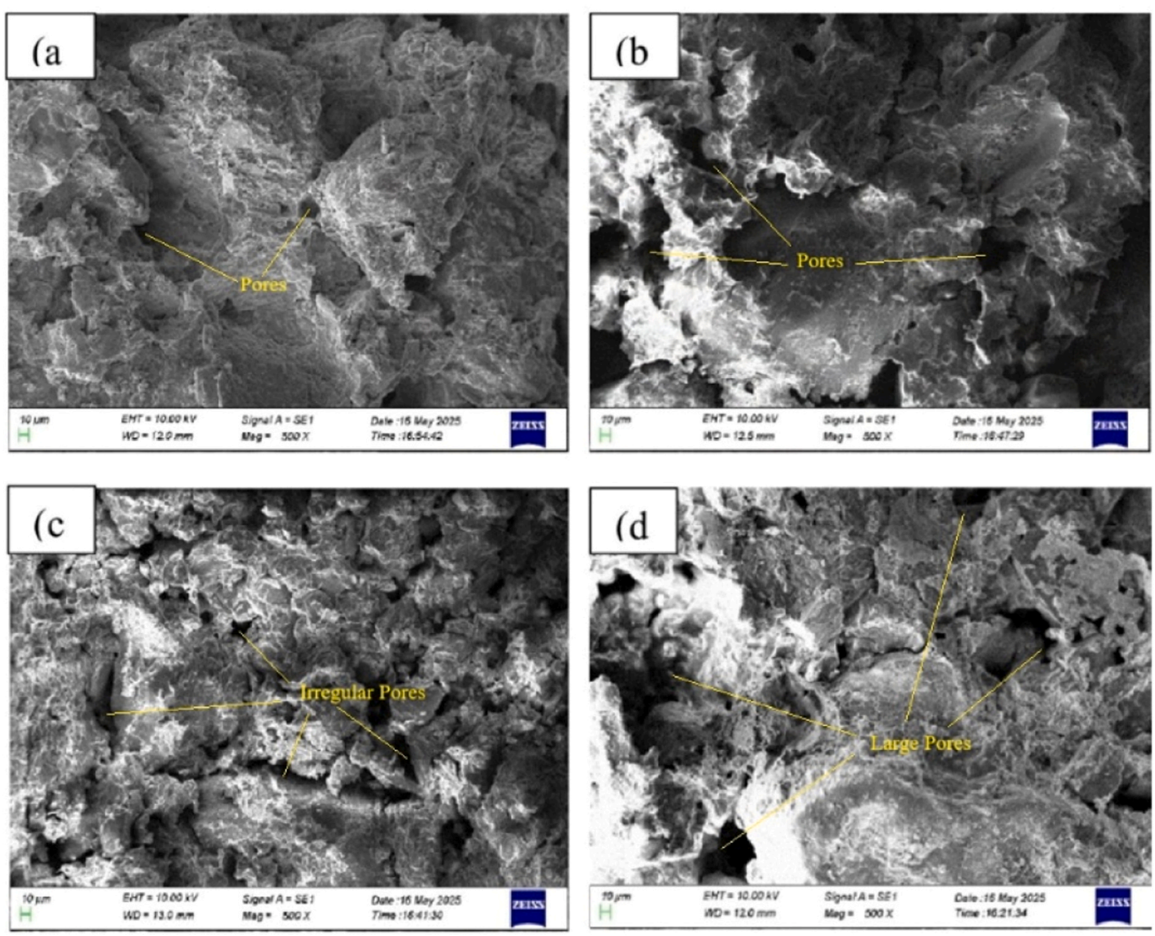

Fig. 10. Image of surface morphology of studied fired brick samples (500X magnification) a)KA3 brick, b)JE1 brick, c) NA1 brick, d) KB1 brick.

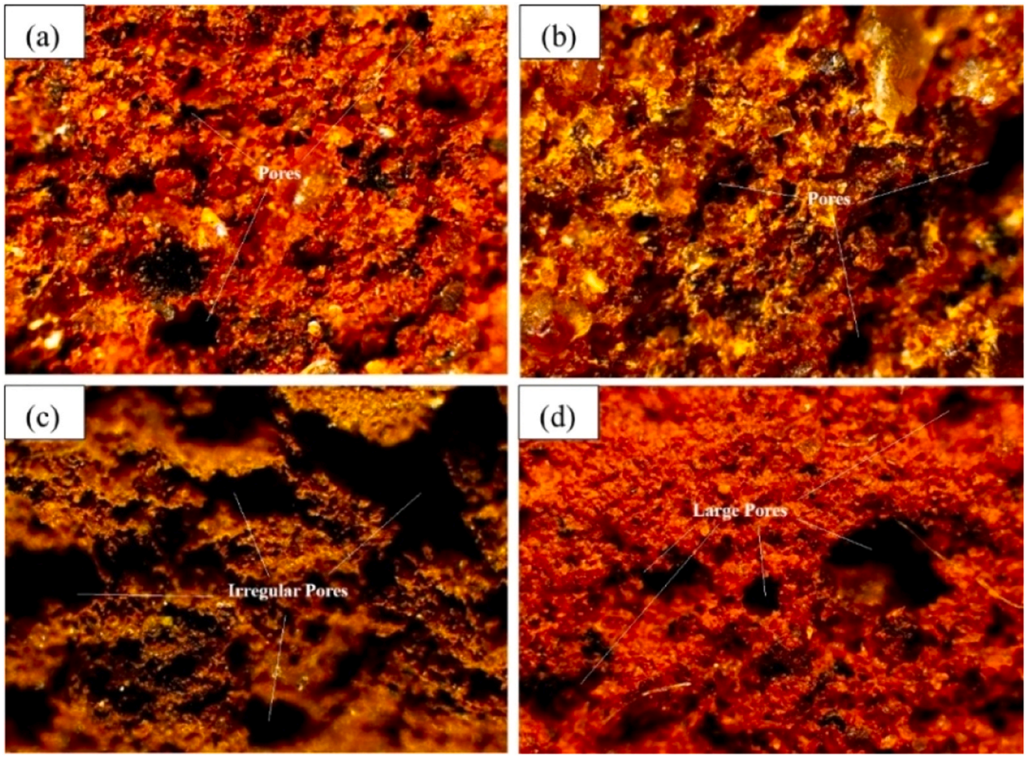

Fig. 11. Microscope images of studied fired brick samples (40X magnification) a)KA3, b)JE1, c)NA1, d)KB1 bricks.

Table 3
SEM-EDX quantification values of ancient bricks and Galkadawala soil.

Elements	KA3	AN3	KU3	JE1	MI	NA1	KB1	Soil
	(Weight%)	(Weight%)	(Weight%)	(Weight%)	(Weight%)	(Weight%)	(Weight%)	(Weight%)
Si K	19.22	23.78	23.49	26.04	22.87	21.23	10.08	13.82
Ti K	0.52	0.77	0.55	0.28	0.42	0.25	3.29	0.19
Al K	13.51	13.69	11.27	11.33	12.75	11.97	7.64	6.34
Fe K	9.43	12	10.06	5.73	7.81	8.72	2.05	2.1
Mn K	0.31	0.2	0.14	0.3	0.04	0.68	1.09	0.05
Mg K	1.1	0.79	1.27	0.58	0.51	1.19	0.7	1.99
Ca K	2.32	1	2.07	3.08	1.74	2.66	0.44	9
Na K	1.08	0.4	0.36	1.97	1.3	1.87	0.39	0.82
K K	1.31	1.42	1.94	0.94	0.52	1.2	0.64	2.96
S K	0.28	0.25	0.32	0.16	0.35	0.33	0.19	0.37
Cl K	0	0.02	0.01	0.05	0	0.11	0	0
Sc K	0.02	0.06	0.02	0.12	0	0.32	0.07	0.04
V K	0	0.06	0.02	0.07	0.03	0.2	0.13	0
Cr K	0.03	0.03	0.03	0.14	0.01	0.46	0.14	0.01
Ni K	0.11	0.15	0.08	0.37	0.02	0.89	0.41	0.1
Cu K	0.07	0.12	0.07	0.42	0.03	0.79	0.3	0.07
Zr L	1.99	0.84	1.46	0.8	0.82	1.23	1.2	1.08
Ba L	0.21	0.47	0.18	0.57	0.05	1.61	0.59	0.07
Ra M	2.05	0.86	1.69	0.85	0.85	1.36	1.25	0.89
C K	8.61	3.34	6.72	3.19	5.81	5.89	4.77	10.37
O K	39.13	39.75	40.19	43.01	44.6	37.05	29.56	52.7
Compressive Strength (N/mm)	9.78	8.7	8.06	7.39	5.96	5.66	2.68	

composition and the Galkadawala soil sample. This may be attributed to the presence of sulfur-bearing minerals in the original clay source or the formation of secondary sulfate phases. However, it should be noted that sulfur behavior in fired materials is complex, as sulfur may be partially volatilized during firing and subsequently reintroduced through post-depositional processes. During the firing, sulphate is retained more effectively when the clay is fired in a less oxidising atmosphere or clay contains appreciable gypsum [61]. Therefore, the elevated sulfur content in ancient bricks likely reflects both the mineralogy of the raw clay and the specific firing conditions used in their production.

These compositional trends suggest that ancient brickmakers may have controlled firing temperatures and utilized the mineralogy of local clays, resulting in bricks with relatively increased alumina content, reduced volatile oxides, and high-temperature silicate phases that may have contributed to their long-term durability and strength.

3.6. *Microstructural characteristics and mechanical performance*

The SEM and elemental mapping analyses were used as qualitative microstructural evidence to support the geochemical and mineralogical

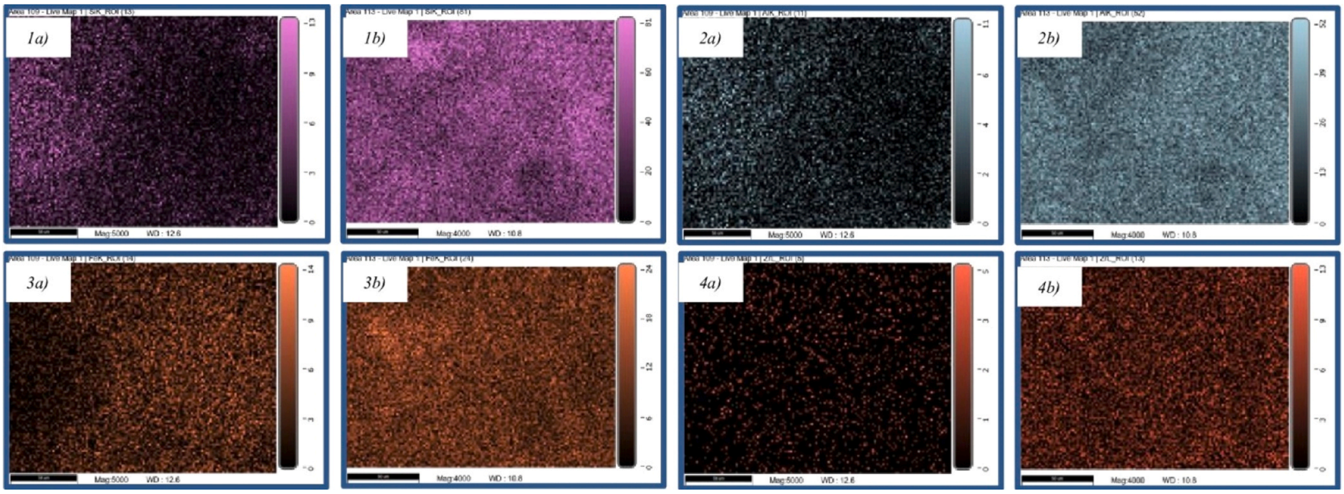

Fig. 12. Map of elemental concentration in KB1(a) brick and KA3(b) brick, 1a,b - Si, 2a,b – Al, 3a,b – Fe and 4a,b - Zr.

interpretations discussed in the preceding sections. According to Maniatis et al. [62], Scanning Electron Microscopy coupled with Energy Dispersive X-ray Spectrometry (SEM-EDX) offers critical insights into the pore structure and the development of the glassy phase in materials. Leriche et al. [63], stated that continuous heating promotes densification, resulting in reduced porosity, which may also cause residual porosity and the onset of grain growth. This process begins with the formation of necks between particles, followed by the development of cylindrical, interconnected pores. As the temperature increases, these pores gradually transform into more spherical and isolated structures. The SEM micrographs (Figs. 10(a)–10d) reveal clear qualitative differences in pore morphology and matrix densification among the studied samples.

The SEM micrographs (Figs. 10a–10d) and microscope images (Figs. 11(a)-11d) show notable variations in microstructural characteristics among the studied brick samples. The KA3 sample (Figs. 10a, 11a) appears to exhibit a relatively dense and compact structure with well-bonded particles and limited visible pore spaces, suggesting enhanced densification. In contrast, JE1 (Figs. 10b, 11b) shows moderately fused particles with some pore presence, suggesting an intermediate densification. NA1 (Figs. 10c, 11c) displays a more irregular structure with increased pore spaces and less effective particle bonding, while KB1 (Figs. 10d, 11d) appears to contain larger pores and a comparatively less compact microstructure with low densification.

According to Thimothy et al. [64], the compressive strength of brick is affected by the porosity, pore size, and type of crystallization. In this context, the relatively dense and compact microstructure observed in the KA3 sample, compared with the KB1 sample, may be an additional factor contributing to its higher compressive strength. As shown in Table 3, KA3 also contains relatively higher contents of carbon, SiO_2, Al_2O_3, and Fe_2O_3 than KB1, and these compositional differences may have influenced firing behavior and phase development. These oxides contribute to the formation of a strong glassy phase during firing, enhancing the material's overall strength [65]. If vitrification fills or minimizes pore spaces left by burnt-out organics, the resulting brick can be both strong and relatively dense [66]. Accordingly, the higher strength of KA3 may reflect the combined influence of its relatively favorable composition and a denser microstructure.

Elemental mapping was further used to assess whether the distribution of key vitrification-related elements supports the microstructural differences observed in the SEM images. According to Fig. 12, KB1 brick shows substantially lower compressive strength (2.68 MPa) than KA3 sample Elemental mapping indicates that silicon and iron are distributed less uniformly in KB1 (Figs. 12, 1a and 3a), whereas KA3 shows a comparatively more homogeneous distribution of these elements (Figs. 12, 1b and 3b). A similar pattern is observed for aluminium and zircon, which appear more evenly distributed in KA3 (Figs. 12, 2b and 4b) than in KB1(Figs. 12, 2b and 4b). Fe_2O_3 acts as a flux, lowering the melting point of clay minerals and promoting glassy phase formation during firing. The uneven distribution of iron and silicon resulted in incomplete vitrification, leading to weak inter-particle bonding and reduced strength [67]. The observed differences in elemental distribution may influence local vitrification behavior and particle bonding. In KB1, the uneven distribution of key elements such as silicon and iron may have contributed to less uniform densification and weaker inter-particle bonding.

Accordingly, the SEM and elemental mapping results provide qualitative microstructural support for the integrated interpretation that compressive strength was governed by the combined influence of flux-assisted vitrification, firing-induced mineral phase development, matrix densification, and pore morphology.

4. Conclusion

This study presents a comprehensive geochemical characterization of ancient burnt clay bricks from the Anuradhapura archaeological complex, Sri Lanka. This study presents an integrated approach combining geochemical, mineralogical, mechanical, and microstructural analyses to systematically investigate the technological basis of ancient Sri Lankan brick production and performance.

The results suggests that ancient Sri Lankan bricks exhibit a notable degree of material adaptability, whereby variations in raw material composition and firing conditions produced favorable combinations of strength, durability, and microstructural stability. This suggests a form of empirical material optimization, indicating that ancient brickmakers may have intuitively controlled key processing parameters to achieve desirable performance characteristics.

Based on the findings of this study, several key characteristics potentially contributing to the durability and strength of ancient burnt clay bricks can be summarized as follows:

i) Predominantly felsic (dacitic–rhyolitic) clay sources, together with possible heavy mineral contributions and compositional variability across the core, middle, and periphery zones, may have influenced mechanical behavior.
ii) Variation with crustal composition of clay suggest that the periphery area exhibits the highest compositional variability and greater heterogeneity in clay sources compared to the core and middle area samples.

iii) Weathering trends suggest that core area bricks exhibit relatively lower alteration compared to middle and periphery samples, while higher flux content may enhance resistance to weathering by promoting densification and reducing porosity.
iv) The clay used in ancient brick production appears to have been low-refractory and non-calcareous (CaO below 6%), which may have contributed to stable firing behavior.
v) Fluxing oxides (particularly Fe_2O_3, K_2O, and CaO) play a significant role in promoting vitrification and densification during firing while maintaining structural integrity.
vi) The firing conditions of the ancient bricks are estimated to fall within a high-temperature range (approximately 900–1100 °C), based on mineral phase assemblages.
vii) The presence of alumina-rich phases such as mullite and diopside contribute to the improved mechanical performance of the KA3 sample (9.78 MPa). Relatively higher concentrations of trace elements (V, Cu, Zn, and Rb) may influence sintering behavior and glass phase development; however, their role is considered secondary, as mullite formation and densification are primarily governed by firing temperature and alumina content.
viii) The development of a relatively dense microstructure with reduced pore connectivity, contributing to improved mechanical strength and durability.
ix) A more uniform elemental distribution and flux-assisted particle bonding may contribute to higher compressive strength, even in the presence of residual pores.

Overall, the felsic-rich clay provenance, elevated flux content, controlled porosity, high-temperature mineral transformations, and uniform elemental distribution collectively appear to have contributed to the higher compressive strength of the burnt clay bricks. These findings provide valuable insights into traditional material optimization strategies and offer certain degree of guidance for the development of sustainable clay-based construction materials. However, further experimental validation studies are required before direct application to modern material design.

CRediT authorship contribution statement

K.D.H.J. Premarathne: Writing – original draft, Visualization, Methodology, Investigation, Funding acquisition, Formal analysis, Data curation, Conceptualization. **Sansfica M. Young:** Writing – review & editing, Validation, Supervision, Software, Resources, Formal analysis, Data curation. **T. Mendis:** Writing – review & editing, Validation, Supervision, Investigation. M. Rajapaksha: Writing – review & editing, Supervision, Software, Resources. **J.M.I.R.K. Jayasekara:** Resources, Investigation, Data curation. **R.U. Halwatura:** Writing – review & editing, Validation, Supervision, Project administration, Data curation. **A. Kamei:** Validation, Resources, Data curation.

Declaration of Generative AI and AI-assisted technologies in the writing process

During the preparation of this work, the authors used ChatGPT to assist with content organization and improving language, readability and structural editing. After using this tool, the authors thoroughly reviewed and revised the content and take full responsibility for the accuracy and integrity of the published article.

Declaration of Competing Interest

The authors declare that they have no known competing financial interests or personal relationships that could have appeared to influence the work reported in this paper.

Acknowledgements

The authors wish to express their profound gratitude to the Department of Civil Engineering, University of Moratuwa and Department of Earth Sciences, Shimane university for providing the research infrastructure and laboratory facilities necessary for the successful execution of this study. The authors also acknowledge the support of the Department of Archaeology, Sri Lanka, for granting access to ancient brick samples and relevant historical documentation that significantly contributed to the research. Further, the authors acknowledge SLINTEC for supporting this research through access to laboratory facilities and technical guidance.

References

[1] E. Allen, R. Thallon, A.C. Schreyer. Fundamentals of Residential Construction, third ed., John Wiley & Sons, San Francisco, 2017. ISBN 978-1-118-978009.
[2] P.R. Fernando, L.A.D. Madushani, M. Praththana, H.M. Nanayakkara, Synthesis and characterization of clay brick using waste groundnut shell ash, J. Waste Resour. Recycl 1 (2018) 101, https://doi.org/10.15744/2766-5887.1.101.
[3] J. Morton, Basic facts about brickwork 1—Structural brickwork, Struct. Surv. 2 (1) (1984) 17–27, https://doi.org/10.1108/eb006187.
[4] F.M. Fernandes, P.B. Lourenço, F. Castro, Ancient clay bricks: manufacture and properties. in: Natural Stone Resources for Historical Monuments, Springer, Dordrecht, 2010, pp. 29–48, https://doi.org/10.1007/978-90-481-2684-2_3.
[5] P.L. Prematilleke, Architectural practices in ancient Anuradhapura, Archaeol. J. 2 (1985) 32–40.
[6] D.P. Gamlath, Architectural Elements and Construction Technology of the Jethavana Stupa, Sarasavi Publishers, Nugegoda, 2016. ISBN 978-955-31-0636-0.
[7] S.U. Deraniyagala, The Prehistory of Sri Lanka: Part II, Department of Archaeological Survey, Colombo, 1992.
[8] M.P. Ranaweera, Ancient stupas in Sri Lanka – largest brick structures in the world, in: CHS Newsletter, 70, London Construction History Society, 2004. ⟨https://www.stupa.org.nz/imagine/CHSPaper.pdf⟩.
[9] M. Ranaweera, H. Abeyruwan, Materials used in the construction, conservation, and restoration of ancient stupas in Sri Lanka. in: Proceedings of the Second International Congress on Construction History, University of Cambridge, Cambridge, 2006, pp. 2573–2586. ⟨https://www.yumpu.com/en/document/view/12412608/materials-used-in-the-construction-conservation-and-restoration⟩.
[10] M.P.R.N. Gunasinghe, B.A. Karunaratne, Mechanical properties of ancient clay bricks of Jethawana Stupa, Rajarata University, RUSL J. 1 (1) (2013) 15–21. ⟨http://repository.rjt.ac.lk/handle/123456789/21⟩.
[11] M. Mostaghelchi, R. Zahiri, S.H. Miremad, A.G. Ebadi, Use of mica mineral powder in bricks industry to improve the performances, Asian J. Chem. 25 (2013) 9144–9148, https://doi.org/10.14233/ajchem.2013.15053C.
[12] K.L. Rasmussen, G.A. De La Fuente, A.D. Bond, K.K. Mathiesen, S.D. Vera, Pottery firing temperatures: a new method for determining the firing temperature of ceramics and burnt clay, J. Archaeol. Sci. 39 (2012) 1705–1716, https://doi.org/10.1016/j.jas.2012.01.008.
[13] A.C. Dunham, A.S. McKnight, I. Warren, Mineral assemblages formed in Oxford clay fired under different time–temperature conditions with reference to brick manufacture, Proc. Yorks. Geol. Soc. 53 (2001) 221–230, https://doi.org/10.1144/pygs.53.3.221.
[14] M.Ghassemi Kakroudi, E. Yeugo-Fogaing, C. Gault, M. Huger, T. Chotard, Effect of thermal treatment on damage mechanical behaviour of refractory castables: comparison between bauxite and andalusite aggregates, J. Eur. Ceram. Soc. 28 (2008) 2471–2478, https://doi.org/10.1016/j.jeurceramsoc.2008.03.048.
[15] I. Johari, S. Said, B. Hisham, A. Bakar, Z.A. Ahmad, Effect of the change of firing temperature on microstructure and physical properties of clay bricks from Beruas, Malaysia, Sci. Sinter. 42 (2010) 245–254, https://doi.org/10.2298/SOS1002245J.
[16] R.E. Hughes, B.L. Bargh, The weathering of brick; causes, assessment and measurement, US Geological Survey, 1982, pp. 83–272. ⟨https://pubs.usgs.gov/of/1983/0272/report.pdf⟩.
[17] British Standards Institution, BS EN 772-1:2011 – Methods of Test for Masonry Units: Determination of Compressive Strength, BSI, London, 2011. ⟨https://www.astm.org/standards-and-solutions/enterprise-solutions/other-publishers⟩.
[18] P.B. Lourenço, M.F. Francisco, F. Castro, Ancient clay bricks: manufacture and properties, in: Technologies and. Practice in Historic Heritage Structures, Springer, Dordrecht, 2009, pp. 37–53, https://doi.org/10.1007/978-90-481-2684-2_3.
[19] R.L. Rudnick, S. Gao, Composition of the continental crust. in: Treatise on Geochemistry, Elsevier, Oxford, 2005, pp. 1–64, https://doi.org/10.1016/B0-08-043751-6/03016-4.
[20] S.M. McLennan, S. Hemming, D.K. McDaniel, G.N. Hanson, Geochemical approaches to sedimentation, provenance and tectonics, Geol. Soc. Am. Spec. Pap. 284 (1993) 21–40, https://doi.org/10.1130/SPE284-p21.
[21] S.R. Taylor, S.M. McLennan, The Continental Crust: Its Composition and Evolution, Blackwell Scientific, Oxford, 1985. ISBN 0-632-01148-3.
[22] I. Kuleff, R. Djingova, Provenance study of pottery: choice of elements to be determined, Archaeom. / Arch. éoSciences 20 (1996) 57–67, https://doi.org/10.3406/arsci.1996.937.

[23] C.S. Munita, R.P. Paiva, M.A. Alves, P.M.S. Oliveira, E.F. Momose, Provenance study of archaeological ceramic, J. Trace Microprobe Tech. 21 (2003) 697–706, https://doi.org/10.1081/TMA-120025819.

[24] A.J. Finlay, J.M. McComish, C.J. Ottley, C.R. Bates, D. Selby, Trace element fingerprinting of ceramic building material from Carpow and York Roman fortresses manufactured by the VI Legion, J. Archaeol. Sci. 39 (2012) 2386–2397, https://doi.org/10.1016/j.jas.2012.03.002.

[25] R.N. Hiscott, Ophiolitic source rocks for Tectonic-age flysch: trace element evidence, Geol. Soc. Am. Bull. 95 (1984) 1261–1267, https://doi.org/10.1130/0016-7606(1985)96.

[26] H.W. Nesbitt, G.M. Young, Early Proterozoic climates and plate motions inferred from major element chemistry of lutites, Nature 299 (1982) 715–717, https://doi.org/10.1038/299715a0.

[27] O.A. Ogbahon, O.B. Olujinmi, Geochemistry of Maastrichtian clastic sedimentary rocks from western flank of Anambra Basin, Nigeria: implications for provenance, tectonic setting, paleoclimate and depositional paleoenvironment, Int. J. Geosci. 10 (2019) 91–118, https://doi.org/10.4236/ijg.2019.101007.

[28] I. Fierăscu, R.C. Fierăscu, A. Baroi, R. Cîrstea, M. Ion, C. Dima, R.I. Bunghez, Archaeometrical characterization of Romanian Late Bronze Age ceramic fragments, Front. Mater. 8 (2021) 630137, https://doi.org/10.3389/fmats.2021.630137.

[29] R. Abdelrahman, S. Wroński, M. Wojenka, J. Tarasiuk, L. Samek, Integrating X-ray fluorescence and X-ray computed tomography for comprehensive analysis of historical ceramics from the Kraków Upland, Nukleonika 70 (2025) 97–109, https://doi.org/10.2478/nuka-2025-0010.

[30] M.G. Babehuk, C.M. Fedo, Analysis of chemical weathering trends across three compositional dimensions: applications to modern and ancient mafic-rock weathering profiles, Can. J. Earth Sci. (2023), https://doi.org/10.1139/cjes-2022-0053.

[31] I. Rorig-Dalgaard, Possible weathering of the brick matrix when exposed to water, in: Proceedings of the 9th International Masonry Conference, Guimarães, Portugal, 2014. ⟨https://orbit.dtu.dk/files/97010381/Possible_weathering_of_the_brick_matrix_1.pdf⟩.

[32] G. Cultrone, E. Sebastián, K. Elert, M.J. de la Torre, O. Cazalla, C. Rodriguez-Navarro, The influence of mineralogy and firing temperature on the porosity of bricks, J. Eur. Ceram. Soc. 24 (2004) 547–564, https://doi.org/10.1016/S0955-2219(03)00249-8.

[33] M.P. Riccardi, B. Messiga, P. Duminuco, An approach to the dynamics of clay firing, Appl. Clay Sci. 15 (1999) 393–409, https://doi.org/10.1016/S0169-1317(99)00017-X.

[34] Y. Maniatis, M.S. Tite, Technological examination of Neolithic–Bronze Age pottery from central and southeast Europe and from the Near East, J. Archaeol. Sci. 8 (1981) 59–76, https://doi.org/10.1016/0305-4403(81)90012-1.

[35] R.W. Grimshaw. The Chemistry and Physics of Clays and Allied Ceramic Materials, fourth ed, Ernest Benn, London, 1971. ⟨https://urn:lcp:2015.125964.The-Chemistry-And-Physics-Of-Clays-Ed1st:epub:aee4cfd9-94fb-47c0-bb4d-f8f9eee6365f⟩.

[36] W.E. Lee, G.P. Souza, C.J. McConville, T. Tarvornpanich, Y. Iqbal, Mullite formation in clays and clay-derived vitreous ceramics, J. Eur. Ceram. Soc. 28 (2008) 465–471, https://doi.org/10.1016/j.jeurceramsoc.2007.04.018.

[37] T. Martišius, R. Giraitis, Influence of copper oxide on mullite formation from kaolinite, J. Mater. Chem. 13 (2003) 121–124, https://doi.org/10.1039/b206711k.

[38] J.-H. Li, H.-W. Ma, W.H. Huang, Effect of V_2O_5 on the properties of mullite ceramics synthesized from high-aluminum fly ash and bauxite, J. Hazard. Mater. 166 (2009) 1535–1539, https://doi.org/10.1016/j.jhazmat.2008.11.059.

[39] K. Elert, G. Cultrone, C. Rodriguez-Navarro, E. Sebastián Pardo, Durability of bricks used in the conservation of historic buildings—influence of composition and microstructure, J. Cult. Herit. 4 (2003) 91–99, https://doi.org/10.1016/S1296-2074(03)00020-7.

[40] R. Ravisankar, G. Raja Annamalai, A. Naseerutheen, A. Chandrasekaran, M.V. R. Prasad, K.K. Satpathy, C. Maheswaran, Analytical characterization of recently excavated megalithic sarcophagi potsherds in Veeranam village, Tiruvannamalai, India, Spectrochim. Acta A Mol. Biomol. Spectrosc 115 (2013) 845–853, https://doi.org/10.1016/j.saa.2013.06.123.

[41] E. Garzón, L. Pérez-Villarejo, D. Eliche-Quesada, S. Martínez-Martínez, P. J. Sánchez-Soto, Vitrification rate and estimation of the optimum firing conditions of ceramic materials from raw clays: a review, Ceram. Int. 48 (2022) 15889–15898, https://doi.org/10.1016/j.ceramint.2022.02.129.

[42] P.J. Sánchez-Soto, E. Garzón, L. Pérez-Villarejo, D. Eliche-Quesada, Sintering behaviour of a clay containing pyrophyllite, sericite and kaolinite as ceramic raw materials: looking for the optimum firing conditions, Bol. Soc. Esp. Ceram. Vidr. 62 (2023) 26–39, https://doi.org/10.1016/j.bsecv.2022.08.004.

[43] M.U. Rehman, M. Ahmad, K. Rashid, Influence of fluxing oxides from waste on the production and physico-mechanical properties of fired clay brick: a review, J. Build. Eng. 27 (2020) 100965, https://doi.org/10.1016/j.jobe.2019.100965.

[44] M.S. Tite, Ceramic production, provenance, and use—a review, Archaeometry 50 (2008) 216–231, https://doi.org/10.1111/j.1475-4754.2008.00391.x.

[45] M.L. Diko, G.E. Ekosse, S.N. Ayonghe, E.B. Ntasin, Physical characterization of clayey materials from tertiary volcanic cones in Limbe, Cameroon, for ceramic applications, Appl. Clay Sci. 51 (2011) 380–384, https://doi.org/10.1016/j.clay.2010.11.034.

[46] C. Modesto, O. de, M. Hofmann, A. de, T.B. Wermuth, S. Arcaro, F. Raupp-Pereira, O.R.K. Montedo, Decoupling alkali and alkaline-earth oxide effects on pyroplastic deformation in porcelain tiles via engineered frits, Mater. Charact. (2026) 116126, https://doi.org/10.1016/j.matchar.2026.116126.

[47] K.J.M.V.R. Rupasingha, W.E.M.H.P. Ekanayake, K.M.N.W. Jayasundara, M.H.C. B. Malawenna, G.A.Y. Perera, W.M.L.R. Wijerathna, N.W.B.A.L. Udayanga, Evaluation of performance enhancement of clay bricks by incorporating coal fly ash generated from a thermal power plant, Sri Lanka J. Technol. 5 (2024). ⟨https://www.seu.ac.lk/sljot/publication/v5n1/002.pdf⟩. ISSN-2773-6970.

[48] G.O. Akintola, F. Amponsah-Dacosta, S.E. Mhlongo, Geotechnical evaluation of clayey materials for quality burnt bricks, Heliyon 6 (2020), https://doi.org/10.1016/j.heliyon.2020.e05626.

[49] C. Wu, J. Ding, M. Jiang, H. Li, L. Wang, Y. Liao, Comprehensive Study on Chemical and Mineral Composition, Physico-Mechanical Properties and Pozzolanic Activity of Ancient Bricks in Hubei, Buildings 16 (2026) 1190, https://doi.org/10.3390/buildings16061190.

[50] G. Cultrone, C. Rodríguez-Navarro, E. Sebastián, O. Cazalla, M.J. de la Torre, Carbonate and silicate phase reactions during ceramic firing, Eur. J. Mineral. 13 (2001) 621–634, https://doi.org/10.1127/0935-1221/2001/0013-0621.

[51] M.M. Jordán, T. Sanfeliu, C. de la Fuente, Firing transformations of Tertiary clays used in the manufacturing of ceramic tile bodies, Appl. Clay Sci. 20 (2001) 87–95, https://doi.org/10.1016/S0169-1317(00)00044-2.

[52] M.S. Tite, Y. Maniatis, Examination of ancient pottery using the scanning electron microscope, Nature 257 (1975) 122–123, https://doi.org/10.1038/257122a0.

[53] C. Rodriguez-Navarro, K. Kudlacz, E. Ruiz-Agudo, The mechanism of thermal decomposition of dolomite: new insights from 2D-XRD and TEM analyses, Am. Mineral. 97 (2012) 38–51, https://doi.org/10.2138/am.2011.3813.

[54] G. Cultrone, J. Carrillo-Rosúa, Growth of metastable phases during brick firing: mineralogical and microtextural changes induced by the composition of the raw material and the presence of additives, Appl. Clay Sci. 185 (2020), https://doi.org/10.1016/j.clay.2019.105419.

[55] D. Faivre (Ed.), Iron Oxides: From Nature to Applications, Wiley-VCH, Weinheim, 2016, https://doi.org/10.1002/9783527691395.

[56] L. Maritan, I. Angelini, G. Artioli, C. Mazzoli, M. Saracino, Secondary phosphates in the ceramic materials from Frattesina, Rovigo, North-Eastern Italy, J. Cult. Herit. 10 (2009) 144–151, https://doi.org/10.1016/j.culher.2008.01.008.

[57] B. Velde, I.C. Druc, Archaeological Ceramic Materials: Origin and Utilization, Springer, Berlin, 1999. ISBN 978-3642641763.

[58] C. Rodriguez-Navarro, E. Ruiz-Agudo, A. Luque, A.B. Rodriguez-Navarro, M. Ortega-Huertas, Thermal decomposition of calcite: mechanisms of formation and textural evolution of CaO nanocrystals, Am. Mineral. 94 (2009) 578–593, https://doi.org/10.2138/am.2009.3021.

[59] Z. Goffer. Archaeological Chemistry, second ed., John Wiley & Sons, Hoboken, NJ, 2007. ISBN 978-0-471-74327-0.

[60] A.L. Wilson, Elemental analysis of pottery in the study of its provenance: a review, J. Archaeol. Sci. 5 (1978) 219–236, https://doi.org/10.1016/0305-4403(78)90041-9.

[61] R.W.M. Rapi, A.F. Jusoh, M. Saidin, Mineralogical and geochemical properties of bricks from Sungai Batu monuments, Bull. Geol. Soc. Malays. 69 (2020) 149–156, https://doi.org/10.7186/bgsm69202013.

[62] Y. Maniatis, A. Simopoulos, A. Kostikas, Effect of reducing atmosphere on minerals and iron oxides developed in fired clays: the role of Ca, J. Am. Ceram. Soc. 66 (1983) 773–781, https://doi.org/10.1111/j.1151-2916.1983.tb10561.x.

[63] A. Leriche, F. Cambier, S. Hampshire, Sintering of ceramics. Reference Module in Materials Science and Materials Engineering, Elsevier, Amsterdam, 2017, https://doi.org/10.1016/B978-0-12-803581-8.10288-7.

[64] F.W. Thimothy, P.A. Adinife, W.K. Joshua, The effect of burnt clay brick production process on the compressive strength and water absorption properties, SNRU J. Sci. Technol. 13 (2021) 63–70. ⟨https://www.researchgate.net/publication/351233995⟩.

[65] L. Maritan, L. Nodari, C. Mazzoli, A. Milano, U. Russo, Influence of firing conditions on ceramic products: experimental study on clay rich in organic matter, Appl. Clay Sci. 31 (2006) 1–15, https://doi.org/10.1016/j.clay.2005.08.007.

[66] D.A. Emmanuel, Characteristics of Burnt Clay Bricks Containing Polythene and Sawdust as Additives (MSc dissertation), Department of Building, Faculty of Environmental Design, Ahmadu Bello University, Zaria, Nigeria, 2017, ⟨https://kubanni.abu.edu.ng/handle/123456789/10254⟩ (MSc dissertation).

[67] E.J. Bassah, W.K. Joshua, Assessing the correlation between brick properties and firing hours of locally produced clay-burnt bricks in Taraba State, Nigeria, Eur. J. Eng. Technol. Res. 6 (2021), https://doi.org/10.24018/ejeng.2021.6.1.2324.